XLIII CILAMCE
21-25, November, 2022
FOZ DO IGUAÇU – PR – BRAZIL

Theoretical and finite element analysis of a laminated composite pipe under combined axisymmetric loading

Inês Sterphanne G. Freitas[1], Waldy T. Zuniga[1], José Renato M. de Sousa[1]

[1]*Civil Engineering Program, COPPE – Federal University of Rio de Janeiro*
Avenida Pedro Calmon, nº 35 Cidade Universitária, 21941-596, Rio de Janeiro – RJ, Brazil
ines.freitas@coc.ufrj.br, waldy.zuniga@coc.ufrj.br, jrenato@laceo.coppe.ufrj.br

Abstract. An essential aspect of hydrocarbon exploitation in offshore fields is ensuring the integrity of the employed flexible pipes. In deep and ultradeep waters, new materials, structural configurations, and numerical and experimental methodologies are required to obtain viable solutions depending on the operational and environmental conditions. For instance, flexible pipes typically employ steel armors to resist the imposed mechanical loads. However, the dimensions of these armors significantly increase with increasing water depths, frequently causing the overload of the top supporting structures in floating production systems. Moreover, these armors are particularly sensitive to stress corrosion cracking (SCC) when transporting fluids rich in contaminants. Aiming to overcome these difficulties, a viable alternative to the typical flexible pipes is the thermoplastic composite pipe (TCP), which is lighter and insensitive to SCC. Hence, this work investigates the response of a composite pipe to combined axisymmetric loadings with two models: an analytical model based on equilibrium and compatibility equations; and a finite element (FE) model. The responses obtained with both models are compared in a parametric study, where the lay-up of the pipes and the operating temperatures are varied. Finally, the burst pressures of these pipes are predicted following different failure criteria.

Keywords: Thermoplastic composite pipe, finite element model, analytical model, failure criteria.

1 Introduction

Exploiting offshore oil and gas in deep and ultradeep waters, as in the Pre-Salt fields on the Brazilian coast, requires hydrocarbon flow systems composed of risers suspended on floating platforms, which typically work under adverse operational and environmental conditions.

In this context of ultradeep exploitation, the riser weight is of great importance due to the support structures overloading the platform, which demands the installation of large, efficient, and often costly flotation systems. In addition, the marine environment is naturally corrosive, as can be the hydrocarbons transported by risers, which may have contaminants capable of inducing corrosive processes, such as hydrogen sulfide (H_2S) and carbon dioxide (CO_2). Particularly, the stress corrosion cracking (SCC) failure mode caused by CO_2 was notified by the Brazilian National Petroleum Agency (ANP) in 2017 [1] through an alert for this previously unknown failure mode in flexible pipes. Thus, developing technical solutions that reconcile economic feasibility, performance, and safety, among other aspects, is necessary.

Despite several attempts to adequately design flexible pipes for these aggressive environments, thermoplastic composite pipes (TCP) are being considered with great interest, mainly to reduce the loads at the top supporting structures and resist SCC. Moreover, the composite material allows multiple applications by changing the design variables (number of layers, thickness, fiber orientation, types of materials, etc.) according to the specifications and constraints required.

Regarding the TCP design, the laminated pipe is one of the few composite structural configurations for which an

exact elasticity solution is available. Herakovich [2] presents the analytical solution for mechanical (tensile, torsion, internal and external pressure) and thermal loads. Xia et al. [3] studied composite pipes with multiple filament-wound layers under internal pressure and presented an exact elastic solution for stresses and strains based on three-dimensional anisotropic elasticity. Bakaiyan et al. [4] derived an elastic solution for stresses and strains of a thermoplastic composite pipe (TCP) under internal pressure and temperature gradient. Xing et al. [5] investigated the effects of the wall thickness on the stresses of a filament-wound cylinder under axial tension and internal and external pressure. Hastie et al. [6] analyzed the effect of thermal gradient on the behavior of TCPs with a FE model. Then, Hastie et al. [7] studied a TCP subjected to combined mechanical and thermal loads.
Despite the benefits of composite materials in offshore pipes, their use by the offshore oil and gas industry is still limited because, according to Mintzas et al. [8], there are uncertainties regarding the mechanical response of these pipes and a lack of field experience and regulatory standards. Hence, theoretical models for the stress analysis of composite pipes are highly desirable to predict their response to in-service offshore loadings adequately. Thus, the present work aims to develop analytical and numerical models to analyze the behavior of laminated composite pipes under axisymmetric thermomechanical loads. Firstly, the model proposed by Herakovich [2] is revisited, followed by a succinct description of a FE model. After that, a parametric study is conducted with these models. In this study, the composite laminate characteristics are modified to evaluate their impact on the mechanical response of a TCP under axisymmetric loading. Finally, the main conclusions of this work are established.

2 Analytical model

The analytical formulation assumes a long pipe made of homogeneous orthotropic layers under axisymmetric thermo-mechanical loading [2]. Mechanical loads are applied at the ends of the pipe or are evenly distributed along its length. Moreover, the thermal load assumes a uniform change in temperature.
The adopted coordinate system consists of a set of cylindrical coordinates x-θ-r defined as the global system of the pipe. In addition to this system, there is a set of local coordinates 1-2-3, considered as the principal material coordinate system, defined for each layer (or ply). In this local system, axis 1 is aligned with the fiber direction, axis 2 is in the layer's plane, perpendicular to the fibers, and axis 3 is normal to the plane of the layer and the fibers. Figure 1 illustrates the adopted system. In this figure, *Re* is the external radius of the pipe, *Ri* is the inner radius of the pipe, ϕ is the fiber orientation or winding angle, *N* is the number of the total layers, and *k* is any layer.

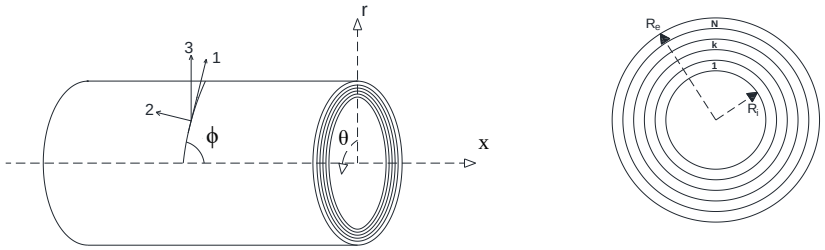

Figure 1. Adopted coordinate system

The strain-displacement relationships in cylindrical coordinates can be described according to Eq. (1) [9].

$$\varepsilon_x = \frac{\partial u}{\partial x}, \qquad \varepsilon_\theta = \frac{1}{r}\left(\frac{\partial v}{\partial \theta} + w\right), \qquad \varepsilon_r = \frac{\partial w}{\partial r},$$
$$\gamma_{\theta r} = \frac{1}{r}\left(\frac{\partial w}{\partial \theta} - v + r\frac{\partial v}{\partial r}\right), \qquad \gamma_{xr} = \frac{\partial u}{\partial r} + \frac{\partial w}{\partial x}, \qquad \gamma_{x\theta} = \frac{\partial v}{\partial x} + \frac{1}{r}\frac{\partial u}{\partial \theta}. \tag{1}$$

where u is the axial displacement, v is the tangential displacement, w is the radial displacement, and ε_x, ε_θ, ε_r, $\gamma_{\theta r}$, γ_{xr}, and $\gamma_{x\theta}$ are the strain components in the global coordinates. Considering only pipes subjected to axisymmetric loads (pressure, axial force, and torsional moment), the displacements, strains, and stresses are independent of θ,

simplifying the relationships shown in Eq. (1)
The generalized Hooke's law, Eq. (2), indicates the proportionality between stress (σ) and strain (ε) components in the local coordinate system, assuming a linear elastic regime.

$$\sigma_i = C_{ij} \cdot (\varepsilon_j - \varepsilon_j^T) \qquad (i, j = 1,...,6) . \tag{2}$$

where the thermal strains are $\varepsilon_j^T = \alpha_j \Delta T$, α_j are the coefficients of thermal expansion of the material, and ΔT is the applied uniform temperature change. Moreover, C is the material's stiffness matrix, also referred to as the elastic constitutive matrix, whose coefficients are given by Eq. (3), considering Poisson's coefficients v and longitudinal and transverse moduli of elasticity, E and G.

$$[C] = \begin{bmatrix} \frac{1-\nu_{23}\cdot\nu_{32}}{E_2\cdot E_3\cdot\Delta} & \frac{\nu_{21}+\nu_{23}\cdot\nu_{31}}{E_2\cdot E_3\cdot\Delta} & \frac{\nu_{31}+\nu_{21}\cdot\nu_{32}}{E_2\cdot E_3\cdot\Delta} & 0 & 0 & 0 \\ \frac{\nu_{21}+\nu_{23}\cdot\nu_{31}}{E_2\cdot E_3\cdot\Delta} & \frac{1-\nu_{13}\cdot\nu_{31}}{E_1\cdot E_3\cdot\Delta} & \frac{\nu_{32}+\nu_{12}\cdot\nu_{31}}{E_1\cdot E_3\cdot\Delta} & 0 & 0 & 0 \\ \frac{\nu_{31}+\nu_{21}\cdot\nu_{32}}{E_2\cdot E_3\cdot\Delta} & \frac{\nu_{32}+\nu_{12}\cdot\nu_{31}}{E_1\cdot E_3\cdot\Delta} & \frac{1-\nu_{12}\cdot\nu_{21}}{E_1\cdot E_2\cdot\Delta} & 0 & 0 & 0 \\ 0 & 0 & 0 & G_{23} & 0 & 0 \\ 0 & 0 & 0 & 0 & G_{13} & 0 \\ 0 & 0 & 0 & 0 & 0 & G_{12} \end{bmatrix} . \tag{3}$$

where Δ is defined as $\Delta = \dfrac{(1-\nu_{12}\cdot\nu_{21}-\nu_{23}\cdot\nu_{32}-\nu_{13}\cdot\nu_{31}-2\nu_{21}\cdot\nu_{32}\cdot\nu_{13})}{E_1\cdot E_2\cdot E_3}$.

The transformation from principal material coordinates to global coordinates is given in Eq (4).

$$\{\sigma\}_x = [T_1]^{-1}[C][T_2]\cdot\left(\{\varepsilon\}_x - \{\varepsilon\}_x^T\right). \tag{4}$$

where the transformation matrices $[T_1]$ and $[T_2]$ are:

$$[T_1] = \begin{bmatrix} m^2 & n^2 & 0 & 0 & 0 & 2mn \\ n^2 & m^2 & 0 & 0 & 0 & -2mn \\ 0 & 0 & 1 & 0 & 0 & 0 \\ 0 & 0 & 0 & m & -n & 0 \\ 0 & 0 & 0 & n & m & 0 \\ -mn & mn & 0 & 0 & m^2 & -n^2 \end{bmatrix}, \qquad [T_2] = \begin{bmatrix} m^2 & n^2 & 0 & 0 & 0 & mn \\ n^2 & m^2 & 0 & 0 & 0 & -mn \\ 0 & 0 & 1 & 0 & 0 & 0 \\ 0 & 0 & 0 & m & -n & 0 \\ 0 & 0 & 0 & n & m & 0 \\ -2mn & 2mn & 0 & 0 & m^2 & -n^2 \end{bmatrix}. \tag{5}$$

where $m = cos\theta$ and $n = sin\theta$. Besides, $\{\varepsilon\}_x^T = \{\alpha\}_x \Delta T$, and $\{\alpha\}_x = [T_2]^{-1}\{\alpha\}_1$.
The axial force equilibrium equation for an N-layer pipe with inside radius R_I and outside radius R_E under axisymmetric loads is:

$$P_x = \int_{R_I}^{R_E} 2\pi\sigma_x r \; dr = 2\pi \sum_{k=1}^{N} \int_{r_k}^{r_{k+1}} \sigma_x^{(k)}(r) r \; dr . \tag{6}$$

Whereas the torque equilibrium equation for an N-layer pipe is:

$$T_x = 2\pi \int_{R_I}^{R_E} \tau_{x\theta} r^2 \; dr = 2\pi \sum_{k=1}^{N} \int_{r_k}^{r_{k+1}} \tau_{x\theta}^{(k)}(r) r^2 \; dr . \tag{7}$$

For a laminated pipe subjected to internal pressure on the internal surface ($r = R_i$) and external pressure on the external surface ($r = R_e$), the stress boundary conditions of Eqs. (8) are valid.

$$\begin{aligned} &\sigma_r(R_i) = -p_i , && \sigma_r(R_i) = -p_i , && \tau_{\theta r}(R_i) = 0 , \\ &\tau_{\theta r}(R_e) = 0 , && \tau_{xr}(R_i) = 0 , && \tau_{xr}(R_e) = 0 . \end{aligned} \tag{8}$$

The exact elasticity solution must also satisfy the conditions for the continuity of stresses and radial displacements at the interfaces between layers. For example, for an *N*-layer pipe with *N-1* interfaces, these conditions represent 2(*N*-1) equations needed for the complete system of simultaneous equations. These continuity conditions can be written in the form shown in Eqs. (9) and (10).

$$w^{(k)} = w^{(k+1)} \qquad \text{(interfaces } k=1, N\text{-}1\text{)}, \tag{9}$$

$$\sigma_r^{(k)} = \sigma_r^{(k+1)} \qquad \text{(interfaces } k=1, N\text{-}1\text{)}. \tag{10}$$

The exact elasticity solution satisfies equilibrium, displacement-strain relationships, compatibility, and boundary conditions for the stated constitutive and loading equations. This formulation was implemented in Matlab® R2019a [10] software.

3 FE model

For the finite element (FE) model of the laminated pipe, the software ANSYS® Mechanical APDL (Ansys Parametric Design Language) - Release 19.1 [11] was used. The modeling was performed as linear elastic analysis using the solid element type SOLSH190, applied to simulate shell structures with a wide range of thicknesses (from thin to moderately thick). This element has eight nodes and 3 degrees of freedom per node (translations in global X, Y, and Z directions), featuring a continuous solid element topology, simplifying the connection to other continuous elements.

Auxiliary elements were used at the end tube to apply the boundary conditions. The TARGE170 element was used to represent a target surface paired with CONTA175 elements to represent the rigid contact between nodes. Furthermore, in all analyzes performed, one end of the tube is clamped, while the opposite end is free only to translate and rotate axially. Figure 2 shows an isometric view of a typical FE model used in this work. Moreover, in all performed analyses, one end of the pipe is clamped, while the opposite end is only free to translate and rotate axially. Figure 2 shows an isometric view of a typical FE model employed in this work.

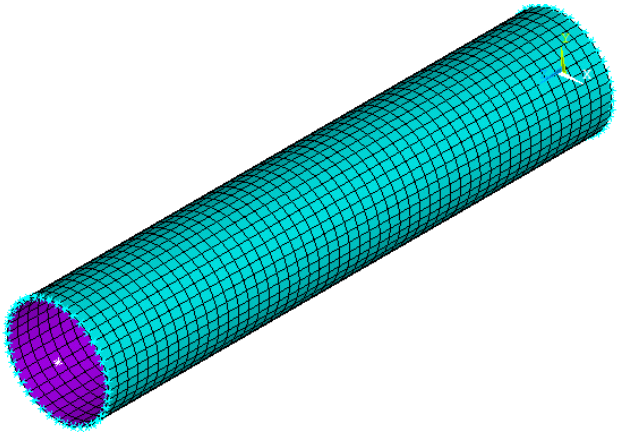

Figure 2. Isometric view of the finite element model

4 Results and discussion

4.1 Case description

The laminated composite pipe used in this paper was presented by Onder et al. [12]. This composite is formed by glass-fiber/epoxy reinforcement plies, whose material properties and strengths are summarized in Tab. 1.

Table 1. Material properties and strengths of the glass-fiber/epoxy reinforcement plies (ONDER et al. [14])

E_{11} [MPa]	$E_{22} = E_{33}$ [MPa]	$G_{12} = G_{13}$ [MPa]	G_{23} [MPa]	$\nu_{12} = \nu_{13}$	ν_{23}	α_1 [1/ºC]	α_2 [1/ºC]
36500	15000	6400	1600	0.24	0.22	7.52E-06	4.78E-05
X_t [MPa]	$Y_t = Z_t$ [MPa]	X_c [MPa]	$Y_c = Z_c$ [MPa]	S [MPa]			
1050	43	938	106	88			

where X_t, Y_t, and Z_t are the tensile strength of the reinforcement ply; X_c, Y_c, and Z_c are the compression strength of the reinforcement ply; E_i, G_i, ν_i, α_i are elastic modulus, shear modulus, Poisson's ratio, and coefficients of thermal expansion, respectively, in principal material coordinates; and S is the shear strength in plane 1-2.

The pipe has an inner diameter of 100 mm and a length of 400 mm and is formed by four plies of 0.4 mm in thickness each, totalizing 1.6 mm. The laminate ply sequences used were $[45º/-45º]_2$, $[55º/-55º]_2$, $[60º/-60º]_2$, $[75º/-75º]_2$, and $[90º/-90º]_2$, evidencing a typical antisymmetrical lay-up (four plies with alternating orientations of ϕ º and - ϕ º, where ϕ is the fiber orientation or winding angle).

The pipe is under internal pressure, axial tensile force associated with this pressure, and change temperature. The FE model mesh has 4960 elements and a total of 9680 nodes.

4.2 Winding angle and temperature effects

Firstly, an internal pressure of 1 MPa with a 0ºC temperature was imposed on the pipe, and the winding angle influence on the induced strains (global coordinates) was verified, as shown in Fig. 3. In addition, the impact of the thermal loading was also verified as shown in Fig. 4. All these results were taken from the inner radius (first ply) of the pipe.

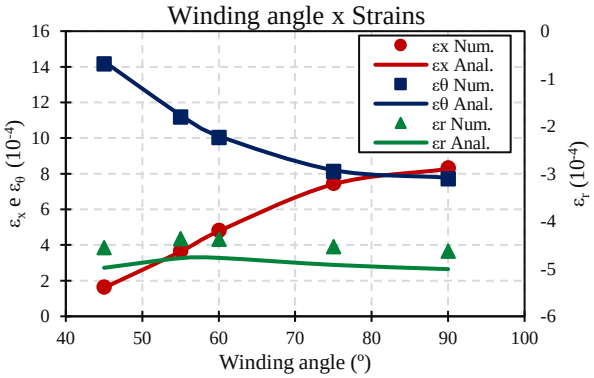

Figure 3. Analytical and numerical responses for strains with different winding angles

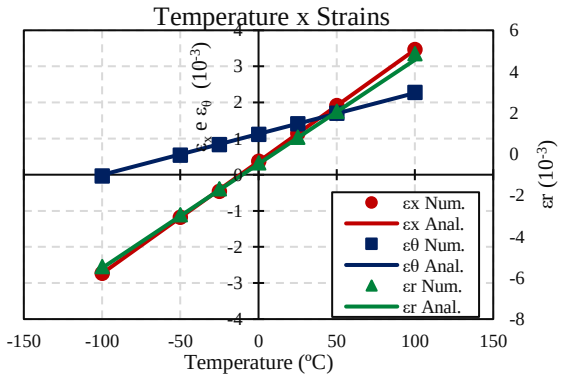

Figure 4. Analytical and numerical responses for strains with different temperatures

Fig. 3 shows that the axial strains were minimal for the smallest winding angle and maximal for the case of 90º, because the mechanical properties of composites with continuous and parallel fibers are highly anisotropic. Thus, as discussed by Callister [13], the reinforcement and strength are maximum in the same fiber direction, and, therefore, the deformations in this direction are minimal. The more aligned the applied loads are in relation to the main direction of the fiber, the smaller the axial deformations will be.. The strength is minimal in the perpendicular fiber direction, and the strains increased. In the hoop direction, the strain is minimal in the fiber orientation at 90º. Still, smaller winding angles increase the resulting strains because these directions are perpendicular to the axial direction, leading to an opposite behavior. However, the winding angle variation did not significantly impact the radial deformations.

The behavior of the pipe under thermal effects, shown in Fig. 4, evidence that the higher the temperature, the higher the resulting strains. Furthermore, it is observed that the axial and radial strains deform in the similar

proportion, while the hoop strain deforms more slowly.
Besides, a significant correlation between analytical and FE models is noted, with very close results. Radial strain results showed a more noticeable deviation. However, they are in minimal quantities.

4.3 Failure criteria

A comparison between different predictions of burst pressures was carried out, considering the failure criteria shown in Tab. 2.

Table 2. Failure criteria for composite materials

Max. Stress [14]	$\frac{\sigma_Y}{Y_T}=1\,;\ \frac{\sigma_X}{X_T}=1\,;\ \frac{\sigma_Y}{Y_C}=1\,;\ \frac{\sigma_X}{X_C}=1\,;\ \frac{\lvert\sigma_S\rvert}{S}=1$
Hashin [15]	$\frac{\sigma_X}{X_T}=1\,;\ -\frac{\sigma_X}{X_C}=1\,;\ \left(\frac{\sigma_Y}{Y_T}\right)^2+\left(\frac{\sigma_S}{S}\right)^2=1\,;\ \left(\frac{\sigma_Y}{Y_C}\right)^2+\left(\frac{\sigma_S}{S}\right)^2=1\,;\ \left(\frac{\sigma_X}{X_T}\right)^2+\left(\frac{\sigma_S}{S}\right)^2=1$
Tsai-Wu [14]	$\frac{\sigma_X^2}{X_T X_C}+\frac{2F_{XY}\sigma_X\sigma_Y}{\sqrt{X_T X_C Y_T Y_C}}+\frac{\sigma_Y^2}{Y_T Y_C}+\frac{\sigma_S^2}{S^2}+\left[\frac{1}{X_T}-\frac{1}{X_C}\right]\sigma_X+\left[\frac{1}{Y_T}-\frac{1}{Y_C}\right]\sigma_Y=1$
Tsai-Hill [16]	$\frac{\sigma_X^2}{X^2}-\frac{\sigma_X\sigma_Y}{X^2}+\frac{\sigma_Y^2}{Y^2}+\frac{\sigma_S^2}{S^2}=1$
Hoffman [16]	$\frac{\sigma_X^2}{X_T X_C}-\frac{\sigma_X\sigma_Y}{X_T X_C}+\frac{\sigma_Y^2}{Y_T Y_C}+\frac{\sigma_S^2}{S^2}+\left[\frac{1}{X_T}-\frac{1}{X_C}\right]\sigma_X+\left[\frac{1}{Y_T}-\frac{1}{Y_C}\right]\sigma_Y=1$

where F_{XY} is assumed to equal -0.5 when test data are absent (Tsai-Wu [14]). σ_x, σ_y, and σ_s are longitudinal, transverse, and in-plane shear stress components in material directions, respectively. In Tsai-Hill [16], X and Y represent the minimum value between tensile (subscript "T") and compressive (subscript "C") strengths.

An iterative process of pressure increment and stress state update was implemented in a Matlab® sub-routine to calculate the burst pressures related to the failure criteria in Tab. 2. Figure 4 presents the burst pressure results obtained for each lay-up, considering the 0ºC temperature case. Moreover, Fig. 5 shows the stress state considering the case of $[55º/-55º]_2$ when it reaches the burst pressure. For this, the lowest burst pressure at this winding angle, defined by Tsai-Hill, was adopted.

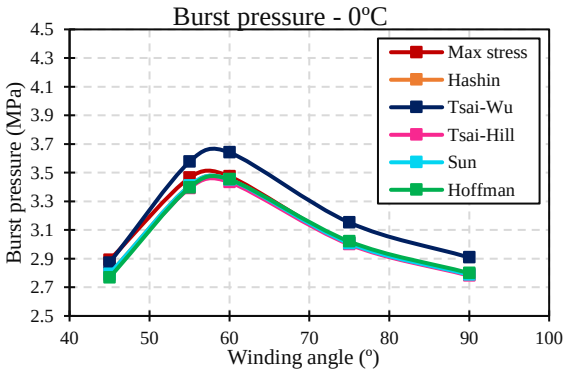

Figure 4. Burst pressure with different winding angles with 0ºC temperature

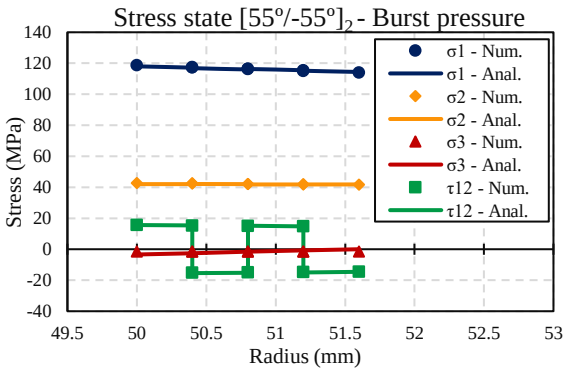

Figure 5. Stress state for $[55º/-55º]_2$ case in burst pressure

Figure 4 shows that all failure criteria presented close burst pressures. Tsai-Wu proved to be the least conservative among these methods. It is also noted that the burst pressure is not proportional to the winding

angle since it starts to decrease after reaching a maximum value. An optimal winding angle (associated with the maximum burst pressure) of 57º is observed in the studied pipe. This value is close to 54.7º, which is the optimal lay angle indicated in some works [17,18].

Fig. 5 also indicates that the analytical and FE models present close results. In addition, it is observed that the stresses are below the limits shown in Tab. 1, and that the failure is occurring in the hoop direction, which has stresses closer to the hoop strength.

5 Conclusions

The implemented analytical and FE models were compared and agreed quite well. Based on the responses of strains about the winding angle, it should be noted that depending on the load combination, knowing that risers are subjected to complex load combinations. Thermal variations tend to cause more significant strains in the composites, and the axial and radial directions undergo higher deformation than the hoop one. The optimal winding angle, which led to the highest maximum burst pressure, was close to 57º.

Acknowledgments. The authors would like to express their thanks for the financial support provided by ANP (Brazilian National Agency of Petroleum, Gas, and Biofuels) and FINEP (Financier of Studies and Projects). The authors also acknowledge the support from FAPERJ (Research Support Foundation of Rio de Janeiro State).

Authorship statement. The authors hereby confirm that they are the sole liable persons responsible for the authorship of this work, and that all material that has been herein included as part of the present paper is either the property (and authorship) of the authors, or has the permission of the owners to be included here.

References

[1] ANP - Agência Nacional do Petróleo. “Safety Alert 001 - CO2 Stress Corrosion Cracking (SCC-CO2)”. *ANP/SSM*, 2017.
[2] Herakovich, C.T. “Mechanics of Fibrous Composites”. *University of Virginia*,1997.
[3] Xia M. Takayanagi, H. Kemmochi, K. “Analysis of multi-layered filament-wound composite pipes under internal pressure”, *Compos. Struct.* 53 (4), 483–491, 2001.
[4] Bakaiyan H, Hosseini H, Ameri E. “Analysis of multi-layered filament-wound composite pipes under combined internal pressure and thermomechanical loading with thermal variations”. *Compos Struct*; 88:532–41, 2009.
[5] Xing J, Geng P, Yang T. “Stress and deformation of multiple winding angle hybrid filament-wound thick cylinder under axial loading and internal and external pressure”. *Compos Struct*; 131:868–77, 2015.
[6] Hastie, J.C. Guz, I.A. Kashtalyan, M. “Effects of thermal gradient on failure of a thermoplastic composite pipe (TCP) riser leg”, Int. J. Press. Vessel. Pip.172. 90–99. 2019.
[7] Hastie, J C, Guz, I A & Kashtalyan, M, “Structural integrity of deepwater composite pipes under combined thermal and mechanical loading*”, Procedia Structural Integrity*, vol. 28, pp. 850-863, 2020.
[8] Mintzas, A.; Hatton, S.; Simandjuntak, S.; Little, A.; Zhang, Z. “An Integrated Approach to the Design of High-Performance Carbon Fiber Reinforced Risers - from micro to macro – scale”. *Deep Offshore Technology Conference*, p. 1-16. Texas, USA: 2013.
[9] FUNG, Y.C. “Foundations of Solid Mechanics”. *Prentice Hall*, New Jersey, 1965.
[10] Ansyc Inc, Mechanical APDL, Release 19.1, Ansys Incorporation, Canonsburg, PA, 2019.
[11] The Mathworks Inc. MATLAB 2019. Natick, MA: The Mathworks Inc; 2019.
[12] Onder A, Sayman O, Dogan T, Tarakcioglu N. “Burst failure load of composite pressure vessels”. *Compos Struct* 2009;89(1):159–66.
[13] Callister JR., W. D., “Fundamentals of Materials Science and Engineering”. 5th ed. John Wiley & Sons: New York, NY, 2001.
[14] Tsai S, Wu E. “A general theory of strength for anisotropic materials”. *J Compos Mater* 1971;5(1):58–80.
[15] Hashin Z, Rotem A. “A fatigue criterion for fiber-reinforced materials”. *J Compos Mater* 1973; 7:448‑64.
[16] Camanho P, “Failure Criteria For Fiber-Reinforced Polymer Composite”; 2002.
[17] Spencer, B., and Hull, D.“Effect of Winding Angle on the Failure of Filament Wound Pipe,” Composites, 9(4), pp. 263–271. 1978.
[18] Eckold, G.“Design and Manufacture of Composite Structures”, McGraw-Hill, Inc., New York, 1994.